Annals of Pharmacy Practice and Pharmacotherapy
ISSN: 3062-4436
2025, Volume 5, Page No: 94-111

Available online at: www.galaxypub.co/page/journals

Galaxy Publication

Galaxy Publication

In Vitro Evaluation and In Vivo Pharmacokinetic Assessment of Intranasal Tadalafil Nanocrystals

Antonio Conti[1], Laura Ricci[1]*, Marco Esposito[1]

[1]Dipartimento di Farmacia, Università degli Studi di Napoli Federico II, Naples, Italy.

***E-mail** ✉ laura.ricci@gmail.com

Received: 28 February 2025; **Revised:** 29 May 2025; **Accepted:** 01 June 2025

ABSTRACT

Tadalafil (TDA), a Biopharmaceutics Classification System (BCS) class II drug, exhibits poor aqueous solubility but high permeability. This study focused on enhancing the bioavailability of poorly soluble TDA through the development of intranasal nanocrystals (NCs). TDA NCs stabilized with polyvinyl alcohol (PVA) demonstrated the smallest particle size and optimal solubility. Formulation F11 measured 196 nm in size, with a polydispersity index (PDI) of 0.21 and a zeta potential of -11.20, showing a 5.5-fold increase in solubility (9.37 ± 0.36 µg/mL) and a 1.6-fold improvement in dissolution rate (50.11 ± 1.69%) compared to pure tadalafil. In vivo studies in animals revealed that the TDA NCs group achieved a maximum plasma concentration (Cmax) of 352.77 ± 35.17 ng/mL and an area under the curve (AUC0∞) of 3377 ± 558 ng·h/mL, significantly higher than the pure TDA group following intranasal administration. In summary, TDA NCs were effectively prepared using the sonoprecipitation method, resulting in notable improvements in both in vitro and in vivo performance, indicating that intranasal delivery of TDA nanocrystals is a promising approach for erectile dysfunction therapy.

Keywords: Pharmacokinetics, Tadalafil, Nanoparticles, Intranasal, Nanocrystals

How to Cite This Article: Conti A, Ricci L, Esposito M. In Vitro Evaluation and In Vivo Pharmacokinetic Assessment of Intranasal Tadalafil Nanocrystals. Ann Pharm Pract Pharmacother. 2025;5:94-111. https://doi.org/10.51847/8J1kgy8yW6

Introduction

Tadalafil (Cialis®) is a selective phosphodiesterase-5 inhibitor (PDE-5I) [1] that has received FDA approval for oral management of erectile dysfunction, pulmonary arterial hypertension, and benign prostatic hyperplasia at recommended doses of 10 mg/day, 40 mg/day, and 5 mg/day, respectively [2]. It is widely regarded as a first-line therapy for erectile dysfunction due to its proven efficacy and safety. This condition primarily affects men over 40 years of age [3] and is defined by the inability to achieve or maintain a penile erection sufficient for successful sexual activity. Factors such as diabetes, hypertension, obesity, smoking, and lower urinary tract disorders are commonly associated with its development and progression [4].

Epidemiological data from the International Consultation Committee for Sexual Medicine (ICCSM) indicate that erectile dysfunction prevalence rises with age, from 1–10% in men under 40 to 50–100% in men above 70 years [5]. The pathogenesis involves a complex interplay of psychological, hormonal, vascular, and neurological mechanisms. Nitric oxide (NO) plays a pivotal role by activating guanylate cyclase, which produces cyclic guanosine monophosphate (cGMP). cGMP then activates protein kinases, especially protein kinase G (PKG), triggering vasodilation in penile tissue. Its action is countered by phosphodiesterases (PDEs), which degrade cGMP, leading to constriction of penile arteries [6]. PDE5 is the dominant PDE in the penis [1], and its inhibition raises cGMP levels, activating PKG and relaxing erectile smooth muscle during sexual arousal [7], forming the molecular basis for PDE5 inhibitor therapy.

As a BCS class II drug, tadalafil exhibits high permeability but poor aqueous solubility, which limits its clinical performance unless solubility and dissolution are enhanced [8]. Its chemical structure is illustrated in **Figure 1**.

One effective approach to overcome low solubility is the development of nanoparticles, typically ranging from 10 to 1000 nm, which increases surface area, accelerates dissolution, and improves oral bioavailability [9, 10].

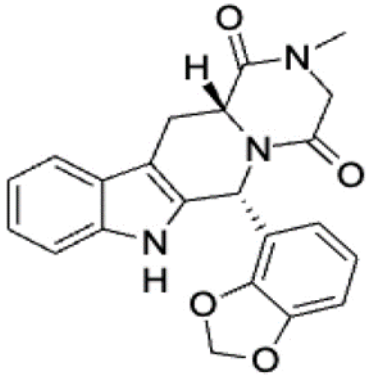

Figure 1. Chemical Structure of Tadalafil.

Nanoparticles can be produced through multiple strategies, including top-down, bottom-up, or hybrid methods combining the two [11]. Top-down approaches focus on breaking down larger particles into nanosized ones via techniques such as wet milling, ultrasonication, or high-pressure homogenization. In contrast, bottom-up strategies rely on the assembly of particles from dissolved drug molecules, where precipitation drives particle formation [12]. Hybrid methods, which integrate both approaches, offer faster production and superior control over particle size reduction [13].

Several techniques have been explored to improve tadalafil's solubility and dissolution, including inclusion complexes [14], solid dispersions [15], and amorphization strategies [16]. Among these, sonoprecipitation represents a combined method, merging anti-solvent precipitation with ultrasonication to generate uniform nanoparticles efficiently [10]. This approach is cost-effective, scalable, and yields nanosuspensions with narrow size distributions [17, 18]. Despite its advantages, limited studies have applied sonoprecipitation to prepare tadalafil nanocrystals.

Nanocrystals (NCs) are drug particles in the crystalline state, typically ranging from 1 to 1000 nm, consisting solely of the active pharmaceutical ingredient without carriers. NCs improve the aqueous solubility of poorly water-soluble compounds [19] and are often formulated as colloidal nanosuspensions stabilized by polymers, surfactants, or their combinations [20]. NCs provide high drug loading and require minimal excipients, reducing potential toxicity while enhancing dissolution, saturation solubility, and oral bioavailability. These improvements can lower the therapeutic dose, decrease side effects, and improve patient compliance [21, 22]. The enhanced solubility arises from the increased surface area of nanosized particles, which accelerates dissolution [23].

The intranasal route has attracted attention as a non-invasive drug delivery method due to its extensive surface area, high vascularization, permeable mucosa, and avoidance of first-pass metabolism, which collectively promote rapid absorption, higher bioavailability, and faster onset of action than oral administration [24, 25]. When combined with NCs, this route increases mucosal contact, prolongs retention time, enhances interaction with tissues or cells, and further improves drug absorption [26].

This study aimed to develop an intranasal formulation of tadalafil NCs to improve solubility, dissolution rate, onset of action, and bioavailability while reducing side effects. The physicochemical properties of the formulations were characterized, and their pharmacokinetic performance was evaluated in a mouse model.

Materials and Methods

Abbreviations

AUC0∞: Total area under the curve, AUMC0∞: Total area under the first moment curve, BCS: Biopharmaceutics Classification System, cGMP: Cyclic guanosine monophosphate, CL/F: Apparent total clearance, Cmax: Maximum plasma concentration, DSC: Differential scanning calorimetry, F: Bioavailability, FDA: Food and Drug Administration, FTIR: Fourier transform infrared spectroscopy, HPLC: High-performance liquid chromatography, IS: Internal standard, LTZ: Letrozole, NCs: Nanocrystals, NO: Nitric oxide, PAH: Pulmonary arterial hypertension, PDE5: Phosphodiesterase 5, PDI: Polydispersity index, PKG: Protein kinase G, PVA:

Polyvinyl alcohol, SEM: Scanning electron microscope, TDA: Tadalafil, tmax: Time to maximum concentration, t0.5: Terminal half-life, λz: Terminal elimination rate constant, XRPD: X-ray powder diffraction.

Materials

Tadalafil (TDA) pure standard (Polpharma, Poland) was generously supplied by Tabuk Pharmaceuticals Co., Jordan. Letrozole (LTZ) as an internal standard (Sigma-Aldrich, Germany), HPLC-grade acetonitrile, and dimethyl sulfoxide (DMSO) were sourced from Fisher, China. Potassium dihydrogen phosphate (AZ Chem, Spain), Tween 80 (polyoxyethylene sorbitan monooleate) (BBC Chemical, China), polyvinyl alcohol 125 kDa (PVA) (Alpha Chemika, India), anhydrous glucose (Sigma-Aldrich, USA), Pluronic F68 (polyoxyethylene-polyoxypropylene block copolymer) (Oakwood Chemical, US), trehalose (Combi Blocks, USA), phosphate-buffered saline (PBS), and deionized water were obtained from Al Takamul Company.

Preparation of tadalafil nanocrystals

Tadalafil NCs were prepared using the sonoprecipitation method. First, 200 mg of TDA was dissolved in 10 mL of DMSO to produce a 20 mg/mL organic solution, which was filtered through a 0.45 µm nylon syringe filter. The aqueous anti-solvent phase consisted of 25 mL DI water containing 2 g of cryoprotectant (glucose or trehalose), with a reference formulation prepared without any cryoprotectant. Stabilizers (Tween 80, PVA, or Pluronic F68) were incorporated at TDA:stabilizer ratios of 1:2 or 1:4 by dissolving 1 g or 2 g of stabilizer in the aqueous phase. Solutions were stirred at 500 rpm for 30 min at room temperature (PVA at 60 °C for 1 h) and filtered through a 0.45 µm nylon membrane.

The organic solution was added dropwise to the aqueous phase at a rate of 0.5 mL/min in a 1:5 volume ratio under magnetic stirring at 500 rpm. The resulting nanosuspension was ultrasonicated for 10 min at 70% amplitude and a cycle of 1 rpm, then stirred overnight to remove DMSO. Nanosuspensions were centrifuged at 16,000 rpm for 30 min, washed three times with DI water, and lyophilized. The dry powders were stored in a desiccator. The control formulation (F0) consisted of raw TDA processed identically without stabilizers or cryoprotectants. Formulation compositions are summarized in **Table 1**.

Table 1. Composition and *in vitro* characterization of tadalafil nanocrystal formulations.

Formulation	Stabilizer	TDA: Stabilizer	Glucose (mg/mL)	Trehalose (mg/mL)	Solubility (mg/mL)	Particle size (nm)	PDI	Zeta potential (mV)
Raw TDA	-	-	-	-	1.71 ± 0.04	-	-	-
F0	0	0	0	0	1.93 ± 0.02	688.80 ± 52.60	0.34 ± 0.10	-15.00 ± 2.40
F1	Tween 80	1:2	0	0	2.08 ± 0.18†	352.00 ± 37.20*	0.29 ± 0.05	-7.17 ± 0.97*
F2	Tween 80	1:2	80	0	2.29 ± 0.01†	307.60 ± 12.60*	0.21 ± 0.01	-5.78 ± 1.58*
F3	Tween 80	1:4	0	0	2.22 ± 0.45	533.80 ± 19.10*	0.30 ± 0.02	-14.76 ± 0.92
F4	Tween 80	1:4	80	0	2.34 ± 0.35	462.20 ± 33.00*	0.34 ± 0.05	-13.13 ± 1.00
F5	Tween 80	1:2	0	80	3.29 ± 0.08†	237.60 ± 2.60*	0.22 ± 0.01	-7.66 ± 2.25*
F6	Tween 80	1:4	0	80	2.92 ± 0.13†	345.80 ± 12.20*	0.32 ± 0.05	-2.99 ± 0.17*
F7	PVA	1:2	0	0	2.76 ± 0.30	341.30 ± 19.60*	0.26 ± 0.01	-21.80 ± 1.41†
F8	PVA	1:2	80	0	2.86 ± 0.37	336.60 ± 7.50*	0.37 ± 0.10	-8.80 ± 2.30*
F9	PVA	1:4	0	0	1.95 ± 0.01†	660.80 ± 4.60	0.35 ± 0.02	-9.69 ± 0.69*
F10	PVA	1:4	80	0	2.49 ± 0.07†	488.60 ± 8.30*	0.42 ± 0.00	-14.00 ± 0.98
F11	PVA	1:2	0	80	9.37 ± 0.36†	196.50 ± 3.30*	0.21 ± 0.01	-11.20 ± 2.13*
F12	PVA	1:4	0	80	4.09 ± 0.03†	359.40 ± 21.40*	0.25 ± 0.01	-9.60 ± 0.69*
F13	Pluronic F68	1:2	0	0	2.13 ± 0.03†	562.40 ± 12.90*	0.34 ± 0.03	-12.30 ± 1.00*
F14	Pluronic F68	1:2	80	0	2.06 ± 0.15	373.90 ± 17.30*	0.25 ± 0.01	-8.60 ± 1.11*
F15	Pluronic F68	1:4	0	0	1.80 ± 0.19	1089.00 ± 73.00†	0.26 ± 0.01	-8.00 ± 0.60*
F16	Pluronic F68	1:4	80	0	2.00 ± 0.06†	779.60 ± 9.00†	0.19 ± 0.01	-6.20 ± 1.50*

F17	Pluronic F68	1:2	0	80	2.74 ± 0.15†	229.20 ± 16.00*	0.37 ± 0.05	-4.42.6 ± 0.34*
F18	Pluronic F68	1:4	0	80	2.14 ± 0.04†	269.90 ± 18.00*	0.36 ± 0.01	-5.04 ± 1.80*

TDA: Tadalafil, PVA: Poly vinyl alcohol, PDI: Polydispersity index. Data: mean ± SD (n = 3). *p-value < 0.05; significantly lower than F0, and †p-value < 0.05 significantly higher than F0.

Characterization of tadalafil nanocrystals

The prepared tadalafil (TDA) nanocrystals (NCs) were systematically characterized for particle size, polydispersity index (PDI), zeta potential, and encapsulation efficiency. Drug stability was also assessed. The formation of nanocrystals was further confirmed using Fourier-transform infrared spectroscopy (FTIR), X-ray powder diffraction (XRPD), differential scanning calorimetry (DSC), and scanning electron microscopy (SEM). Additionally, the solubility and in vitro release profile of TDA from the NCs were evaluated.

Particle size, polydispersity, and zeta potential

The mean particle size, PDI, and zeta potential of the NCs were measured using a Malvern Zetasizer (Malvern Instruments, UK). Lyophilized nanocrystals were dispersed in deionized (DI) water before analysis. Zeta potential values were calculated using the Zetasizer Nano software. All measurements were conducted in triplicate.

Saturation solubility

Saturation solubility of pure TDA and the nanocrystal formulations was determined in DI water at 37 °C over 48 hours. Excess TDA or NCs were added to 10 mL DI water in Erlenmeyer flasks and agitated using a shaking water bath. The suspensions were filtered through a 0.45 µm nylon syringe filter, and TDA concentration was quantified using high-performance liquid chromatography with UV detection (HPLC-UV) at 285 nm. Separation was performed on a C18 column (150 mm × 4.6 mm, 5 µm, Fortis, UK) using a mobile phase of potassium dihydrogen phosphate buffer and HPLC-grade acetonitrile (50:50 v/v) at a flow rate of 1.3 mL/min [27]. Calibration curves were linear over 0.39–100 µg/mL ($r^2 = 0.9999$). All measurements were performed in triplicate.

Encapsulation efficiency

A known quantity of lyophilized NCs was dissolved in 10 mL DMSO, and the concentration of TDA was measured using the HPLC-UV method described above. Encapsulation efficiency (%) was calculated as [28]:

$$Encapsulation\ ef\ ficiency\% = \frac{Actual\ amount}{Theortical\ amount} \times 100\% \quad (1)$$

In vitro dissolution

Dissolution studies of pure TDA and selected NCs were conducted using a USP II (paddle) apparatus with modifications. Samples containing 5 mg of TDA (or equivalent NCs) were added to 900 mL of 0.156 M phosphate-buffered saline (PBS, pH 7.4) at 37 ± 0.5 °C, stirred at 50 rpm. Aliquots (1.5 mL) were withdrawn at multiple time points (0.16, 0.33, 0.5, 0.75, 1, 1.5, 2, 4, 6, 8, 24, 48 h) and replaced with fresh PBS. Samples were filtered (0.45 µm nylon) and analyzed via HPLC-UV. Drug release profiles were plotted as percentage released versus time. All experiments were performed in triplicate.

Fourier-transform infrared spectroscopy (FTIR)

FTIR spectra of TDA, selected stabilizers, NCs, and their physical mixtures were recorded using a Shimadzu FTIR spectrometer (Kyoto, Japan). Physical mixtures were prepared by combining TDA and stabilizer in the same ratio used in the formulations. Samples were mixed with KBr, pressed into disks, and scanned over 400–4000 cm^{-1} to assess chemical compatibility and stability.

X-ray powder diffraction (XRPD)

The crystallinity of TDA, stabilizers, NCs, and physical mixtures was examined using an Ultima IV X-ray diffractometer (Rigaku, Japan) with cobalt radiation at 40 kV and 40 mA. Diffraction patterns were recorded over 2θ angles of 3°–60° with a step size of 0.02° at 3°/min in step-scan mode to evaluate the structural integrity and stability of the formulations.

Differential scanning calorimetry (DSC)

The thermal behavior of TDA, stabilizers, NCs, and their physical mixtures was analyzed using a DSC-204 (Netzsch, Germany). Approximately 3 mg of each sample was placed in aluminum pans and heated from ambient temperature to 400 °C at 10 °C/min under a nitrogen atmosphere. An empty pan served as a reference. DSC confirmed the thermal stability and compatibility of TDA with formulation components.

Morphology analysis

The surface morphology of the lyophilized NCs was examined using a FEI Quanta 450 FEG SEM. Samples were mounted on metal stubs and coated with gold under vacuum before imaging.

Stability and aging studies

The optimized TDA NC formulation was stored at room temperature (25 ± 0.5 °C) and under accelerated conditions (4 ± 0.5 °C and 40 ± 0.5 °C). Particle size, PDI, and saturation solubility were measured on days 1, 30, 60, and 90 following the previously described methods to evaluate stability over time.

Animals

All animal experiments were conducted in accordance with the guidelines set by the Animal Care and Use Committee (ACUC) of Jordan University of Science and Technology (JUST, Jordan). Male Sprague Dawley (SD) rats (n = 8; 300–350 g) were sourced from the JUST animal facility. The rats were maintained under controlled conditions with a temperature of 25 ± 2 °C, a 12-hour light/dark cycle, and approximately 50% relative humidity. Prior to the start of the study, the animals were acclimated to laboratory conditions for one week and provided unrestricted access to water and standard chow. Experimental procedures strictly adhered to ACUC guidelines. Rats were randomly assigned to two groups (n = 4 each). The first group received the selected TDA formulation intranasally, while the second group received pure TDA via the same route. The Tadalafil dose was determined using the following equation:

$$\text{Animal dose (mg/kg)} = \text{HED} \times (Km_{\text{human}} \div Km_{rat}). \quad (2)$$

where HED is the human equivalent dose in mg/kg, with Km_human = 37 and Km_rat = 7 [29]. This calculation resulted in an administered dose of 4 mg/kg TDA for all groups.

Pharmacokinetic study

Rats in the first group (n = 4) received a single intranasal dose of TDA NCs (F11) equivalent to 4 mg/kg. The nanocrystal powder was suspended in 100 µL of 2% PEG400 and 0.02% Tween 80, with 50 µL delivered into each nostril using a micropipette [30, 31]. Blood samples (150–200 µL) were collected into EDTA-treated tubes at 1, 2, 4, 5, 6, 6.5, 7, 7.5, 8, and 24 h. The second group (n = 4) received a single intranasal dose of pure TDA (4 mg/kg) in the same vehicle, with sampling at 1, 2, 3.5, 4.5, 5, 6, 7, 8, and 24 h. Plasma was separated by centrifugation at 600 × g for 15 minutes and stored at –80 °C until analysis. Drug quantification was performed via HPLC-UV at 285 nm using a C18 column (150 mm × 4.6 mm, 5 µm; Agilent, US) at 35 °C. The mobile phase consisted of potassium dihydrogen phosphate buffer and HPLC-grade acetonitrile (63:37 v/v) with a flow rate of 1.3 mL/min. Plasma extraction was performed using direct precipitation: 120 µL of HPLC-grade acetonitrile containing the internal standard (LTZ, 40 µg/mL) was added to each plasma tube, vortexed for 30 seconds, and centrifuged at 16,000 rpm for 5 minutes. Then, 150 µL of the supernatant was collected and reconstituted with 50 µL of DI water. The method was validated for specificity, selectivity, recovery, precision, accuracy, and linearity over 10–10,000 ng/mL according to FDA guidelines (2022) [32].

Pharmacokinetic analysis

Non-compartmental pharmacokinetic analysis was conducted using WinNonlin 5.3 (Pharsight Corp., Palo Alto, CA, USA). Cmax and Tmax were obtained directly from the concentration-time profiles. The total area under the curve (AUC_0^∞) was calculated using the linear trapezoidal method. Mean residence time (MRT) was determined as MRT = $AUMC_0^\infty / AUC_0^\infty$, where $AUMC_0^\infty$ is the area under the first moment curve. The apparent volume of distribution during the terminal phase (V_z / F) was calculated as V_z / F = Dose / ($AUC_0^\infty \times \lambda_z$), with λ_z representing the terminal elimination rate constant derived from the slope of the terminal phase. Apparent clearance was computed as CL / F = Dose / AUC_0^∞. The terminal half-life (t_0.5) was calculated using $t_{0.5} = 0.693 / \lambda_z$.

Statistical analysis

Data were analyzed using GraphPad Prism 9.4.3. Unpaired t-tests were applied, with p-values < 0.05 considered statistically significant. Results are presented as mean ± SD (n = 3–4).

Results and Discussion

Particle size, polydispersity index, and zeta potential

The particle size, polydispersity index (PDI), and zeta potential of the control (F0) and various TDA NC formulations are summarized in **Table 1**. The formulations exhibited notable variation in size and surface charge. F11 showed the smallest particle size (196.50 ± 3.30 nm) with a PDI of 0.21 ± 0.01, while F15 displayed the largest size (1089.00 ± 73.00 nm) with a PDI of 0.26 ± 0.01. The control formula F0 had a particle size of 688.80 ± 52.60 nm and a PDI of 0.34 ± 0.10. Except for F15, all formulations were nanosized (<1000 nm) with particle sizes ranging from 196.50 ± 3.30 to 779.60 ± 9.00 nm and PDI values between 0.19 ± 0.01 and 0.42 ± 0.00. Unpaired t-test analysis indicated that all formulations had significantly smaller sizes than F0, except F9, F15, and F16, which were significantly larger ($p < 0.05$). Increasing the stabilizer concentration generally led to larger particle sizes.

Comparing stabilizers, PVA-stabilized NCs had significantly smaller sizes than those stabilized with Tween 80 (e.g., F2 vs. F8, F3 vs. F9, F5 vs. F11) and Pluronic F68. **Figure 2** illustrates the impact of stabilizer type on particle size. Differences in particle size can be attributed to stabilizer efficiency in controlling NC growth. Key factors include the interactions between the drug surface and stabilizer (hydrogen bonding, hydrophilic/hydrophobic, or ionic interactions), the steric hindrance imposed by the polymer chain, and the proportion of NC surface covered by the stabilizer [33, 34]. PVA contains abundant hydroxyl groups, which form hydrogen bonds with TDA's carbonyl group, enhancing polymer adsorption on the hydrophobic drug surface and providing combined electrostatic and steric stabilization to inhibit crystal growth and aggregation [35–37]. Tween 80 primarily offers electrostatic stabilization, reducing Van der Waals-driven aggregation, which may be less effective for TDA [38]. The higher viscosity of PVA also limits particle mobility, reducing collision frequency and particle growth [39]. Pluronic F68, a block copolymer of hydrophobic polypropylene oxide (PPO) and hydrophilic polyethylene oxide (PEO), interacts with the drug surface via PPO while providing steric hindrance through PEO. Despite this, larger particles were observed compared to PVA-stabilized NCs [38, 40].

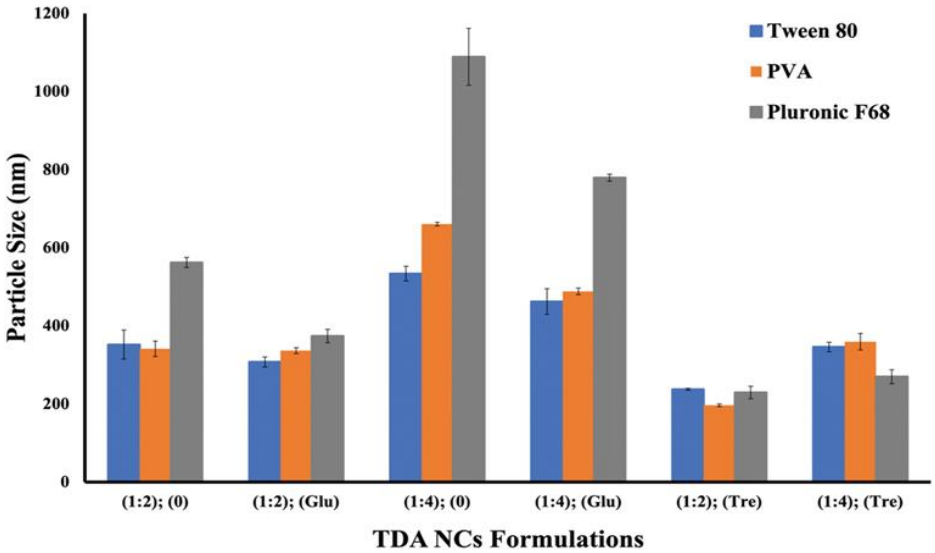

Figure 2. Influence of stabilizer type on tadalafil nanoparticle (TDA NCs) size. The y-axis represents [(TDA: stabilizer); (cryoprotectant)]. Glu: glucose, Tre: trehalose. Values are shown as mean ± SD (n = 3).

Higher concentrations of stabilizers were associated with an increase in nanoparticle size and a concomitant decline in solubility. This effect can be explained by the aggregation (flocculation) of nanoparticles occurring at elevated stabilizer levels, which has been documented in previous studies [41, 42]. At such high concentrations, the stabilizers were less effective at maintaining nanoparticle stability. The relationship between stabilizer concentration and the resulting TDA NC size is depicted in **Figure 3**.

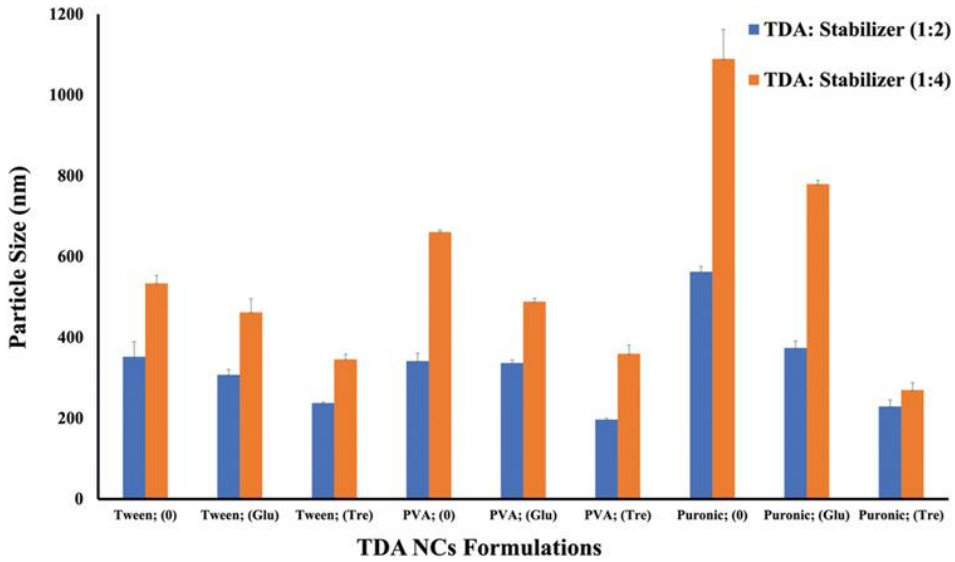

Figure 3. Influence of stabilizer concentration on the particle size of tadalafil nanoparticles (TDA NCs). The y-axis represents [Stabilizer; (cryoprotectant)]. Glu: glucose, Tre: trehalose. Values are expressed as mean ± SD (n = 3).

It was observed that formulations prepared with cryoprotectants generally exhibited smaller particle sizes compared to those without cryoprotectants. The primary role of cryoprotectants is to minimize nanoparticle aggregation that occurs during the freeze-drying process. Notably, trehalose proved more effective than glucose in reducing particle size, which can be attributed to its lack of internal hydrogen bonding, low hygroscopicity, minimal chemical reactivity, and higher glass transition temperature (Tg) [43]. In contrast, glucose was less capable of protecting the TDA NCs from aggregation, as indicated by the larger average particle size observed at equivalent stabilizer concentrations. Additionally, competition between stabilizers and cryoprotectants for adsorption on the nanoparticle surface may explain why certain formulations failed to maintain stability in the presence of either glucose or trehalose.

The polydispersity index (PDI) of the nanoparticles ranged from 0.19 ± 0.01 to 0.42 ± 0.00, indicating a relatively narrow particle size distribution, which is important for maintaining physical stability and preventing particle growth [44]. Zeta potential values ranged from -2.99 ± 0.17 to -21.80 ± 1.41 mV, while the control formula (F0) had a zeta potential of -15.00 ± 2.40 mV. Formulations containing glucose or trehalose exhibited significantly lower zeta potentials compared to those without cryoprotectants. Although non-ionic stabilizers such as PVA, Tween 80, and Pluronic F68 partially mask the negative charge of TDA, adsorption of the cryoprotectant onto the nanoparticle surface further shields this charge [45].

Saturation solubility

Pure TDA demonstrated a solubility of 1.71 ± 0.04 µg/mL in DI water at 37 °C, which was not significantly different from the control formula (1.93 ± 0.02 µg/mL). The solubility results for the prepared NCs are presented in **Table 1**. Among all formulations, F11 exhibited the highest solubility (9.37 ± 0.36 µg/mL), representing an approximate 5.5-fold improvement over pure TDA, whereas F15 showed the lowest solubility (1.8 ± 0.19 µg/mL). In general, PVA-stabilized NCs achieved higher solubility compared to those stabilized with Tween 80 or Pluronic F68 [46].

The enhanced solubility of NCs can be attributed primarily to the reduction in particle size, which increases the surface area and improves wettability, facilitating greater interaction with the dissolution medium [47]. Stabilizers may further contribute to solubility through wetting and solubilizing effects. Differences in solubility between similarly sized particles may also arise from a partial reduction in crystallinity of the TDA NCs. As stabilizer concentration increases, solubility tends to decrease, reflecting the associated increase in particle size [42]. Terayama *et al*. (2004) similarly reported that flocculation occurs at high stabilizer concentrations, where micelle formation leaves drug particles insufficiently protected, reducing solubility [41].

Moreover, formulations containing trehalose displayed higher solubility than others, likely due to improved re-dispersibility—the ability of dried nanoparticles to regain their original dispersion in aqueous media, which is strongly influenced by the type and amount of cryoprotectant used [48]. F11, having the smallest particle size and

highest solubility, was therefore selected for subsequent detailed characterization. **Figure 4** illustrates the effect of stabilizers on the saturation solubility of TDA NCs.

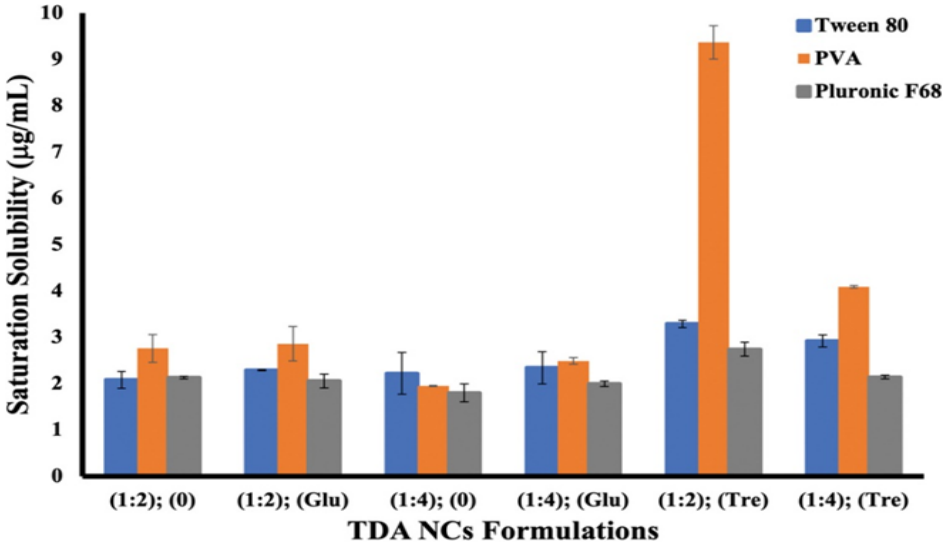

Figure 4. Influence of stabilizer type on the saturation solubility of tadalafil nanoparticles (TDA NCs). The y-axis represents [(TDA: stabilizer); (cryoprotectant)]. Glu: glucose, Tre: trehalose. Values are expressed as mean ± SD (n = 3).

Encapsulation efficiency

The encapsulation efficiency (EE%) of the TDA NCs was determined in triplicate for all formulations. The results showed that EE% values ranged from 98.90 ± 2.8% to 103.1 ± 2.7%, with F11 exhibiting an encapsulation efficiency of 99.16 ± 4.91%. Statistical analysis using a t-test indicated no significant difference between the measured drug content and the theoretical amount for any of the formulations, confirming efficient drug entrapment.

In vitro dissolution study

The dissolution behavior of pure TDA and the selected formulation (F11) was evaluated in PBS, as illustrated in **Figure 5**. F11 demonstrated 50.11 ± 1.69% drug release at 6 hours and 57.70 ± 4.6% at 48 hours, whereas pure TDA released 30.90 ± 2.65% and 45.30 ± 2.75% over the same periods. This indicates a marked enhancement in the release profile for F11 compared to the pure drug. Specifically, F11 showed a 1.66-fold and 1.3-fold increase in drug release relative to pure TDA at 6 hours and 48 hours, respectively, highlighting the improved dissolution characteristics of the nanocrystal formulation.

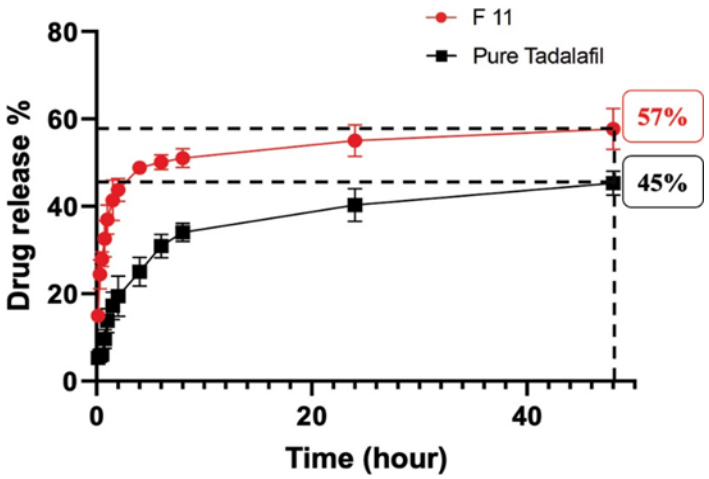

Figure 5. Dissolution profiles of pure TDA and TDA NC (F11) in PBS at 37 °C over 48 hours. Data are expressed as mean ± SD (n = 3).

FTIR analysis

Fourier-transform infrared (FTIR) spectroscopy was employed to investigate potential chemical interactions or incompatibilities between TDA and the stabilizer by analyzing pure TDA, PVA, their physical mixture, and the optimized nanocrystal formulation (F11). The FTIR spectra are shown in **Figure 6**.

For pure TDA, characteristic absorption peaks were observed at 748 cm^{-1} (benzene ring), 1041 cm^{-1} (C–O–C stretching), 1435 cm^{-1} (C–N stretching), 1651 cm^{-1} (aromatic C=C), 1682 cm^{-1} (C=O carbonyl), 2904 cm^{-1} (C–H stretching), and 3327 cm^{-1} (N–H stretching) [49]. PVA displayed a broad band at 3000–3700 cm^{-1} corresponding to O–H stretching, 2360 cm^{-1} for CH_2 stretching, 1700 cm^{-1} for C=O stretching, 1650 cm^{-1} for C=C stretching, 800 cm^{-1} for C–C stretching, and 486 cm^{-1} for C–O bending [50].

The physical mixture spectrum contained peaks corresponding to both TDA and PVA. A slight reduction in TDA peak intensity was noted, likely due to dilution by PVA, indicating no significant chemical interaction between TDA and PVA in the mixture.

In the FTIR spectrum of F11, all characteristic TDA peaks were retained. The N–H stretching peak at 3327 cm^{-1} shifted slightly to 3325 cm^{-1} with reduced intensity, suggesting possible hydrogen bonding between TDA's amine group and PVA's hydroxyl groups, consistent with polymer–drug interactions reported by Bhokare *et al*. [51]. Similarly, the C–O–C stretching peak shifted from 1041 cm^{-1} to 1044 cm^{-1}, further supporting hydrogen bond formation between TDA and PVA, as previously observed by Athokpam *et al*. [52]. No new peaks appeared in the F11 spectrum, confirming that no chemical reactions occurred between TDA and PVA during nanocrystal formation.

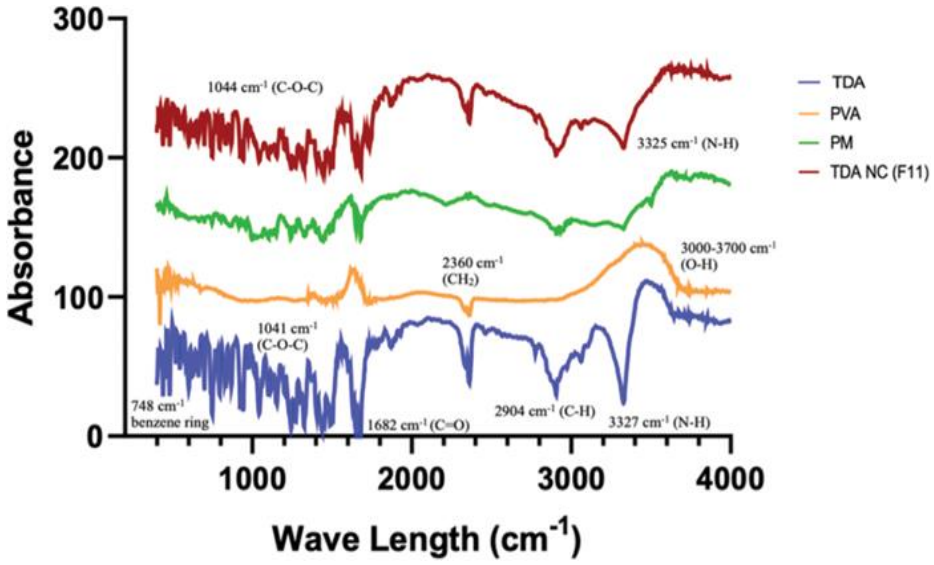

Figure 6. FTIR spectra of pure TDA, PVA, the physical mixture (PM), and TDA nanocrystals (F11).

DSC analysis

Differential scanning calorimetry (DSC) was employed to investigate the thermal properties of pure TDA, PVA, their physical mixture, and the optimized nanocrystals (F11), as presented in **Figure 7**. Pure TDA exhibited a sharp endothermic peak at 302 °C, which corresponds to its melting point in the crystalline form [53]. PVA displayed an endothermic peak at 194 °C, consistent with its reported melting temperature [54].

The DSC thermogram of the physical mixture showed both peaks at 194 °C and 302 °C, indicating that the melting points of PVA and TDA remained distinct, suggesting no thermal incompatibility between the drug and the polymer. Interestingly, the F11 nanocrystals exhibited a single, broadened endothermic peak at 270 °C. This downward shift in melting temperature likely results from a combination of reduced particle size and a partial loss of crystallinity in the TDA nanocrystals, consistent with previous observations for drug–polymer nanocomposites [51].

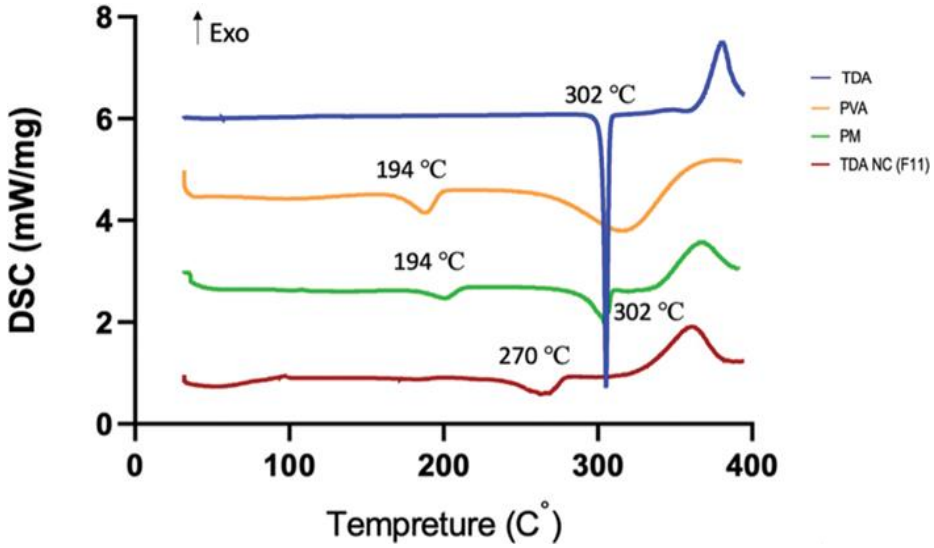

Figure 7. DSC thermograms of pure TDA, PVA, the physical mixture (PM), and tadalafil nanocrystals (TDA NC; F11).

XRPD analysis

X-ray powder diffraction (XRPD) was used to examine the crystalline characteristics of the prepared nanocrystals. The XRPD patterns for pure TDA, PVA, their physical mixture, and F11 are shown in **Figure 8**. Pure TDA displayed sharp and well-defined peaks at 2θ values of 7, 10, 14, 16, 18, 22, and 24°, which are indicative of its crystalline structure [55]. In contrast, PVA exhibited broad diffraction peaks, reflecting its amorphous nature [56]. In the physical mixture, the characteristic TDA peaks were still visible but with reduced intensity, likely due to dilution by PVA. The XRPD pattern of F11 retained the primary diffraction peaks of TDA; however, their intensities were further diminished. This reduction is likely a result of both decreased particle size and partial alteration of the crystallinity of TDA, possibly influenced by interactions with PVA in the nanocrystal formulation. These observations align well with the DSC findings and the morphological changes noted in the SEM analysis.

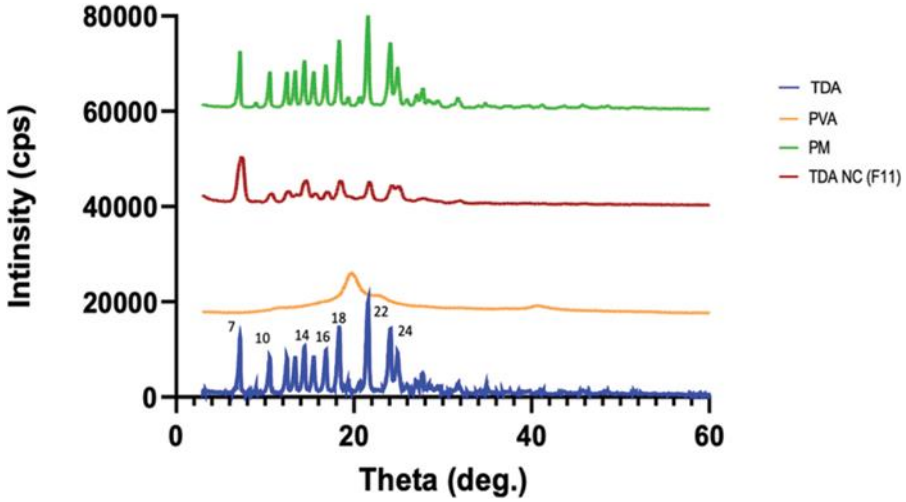

Figure 8. XRD patterns of pure TDA, PVA, the physical mixture (PM), and tadalafil nanocrystals (TDA NC; F11).

SEM analysis

Scanning electron microscopy (SEM) was employed to assess the morphology of pure TDA and the optimized nanocrystals (F11), as illustrated in **Figure 9**. Pure TDA appeared as a heterogeneous mixture of needle-like and cubic crystals, exhibiting a broad particle size distribution, with smaller particles forming noticeable aggregates. In contrast, the F11 nanocrystals stabilized with PVA displayed a more uniform distribution of needle-like

structures, with significantly reduced particle size compared to the unprocessed TDA, indicating effective size reduction and improved dispersion achieved through nanocrystal formulation.

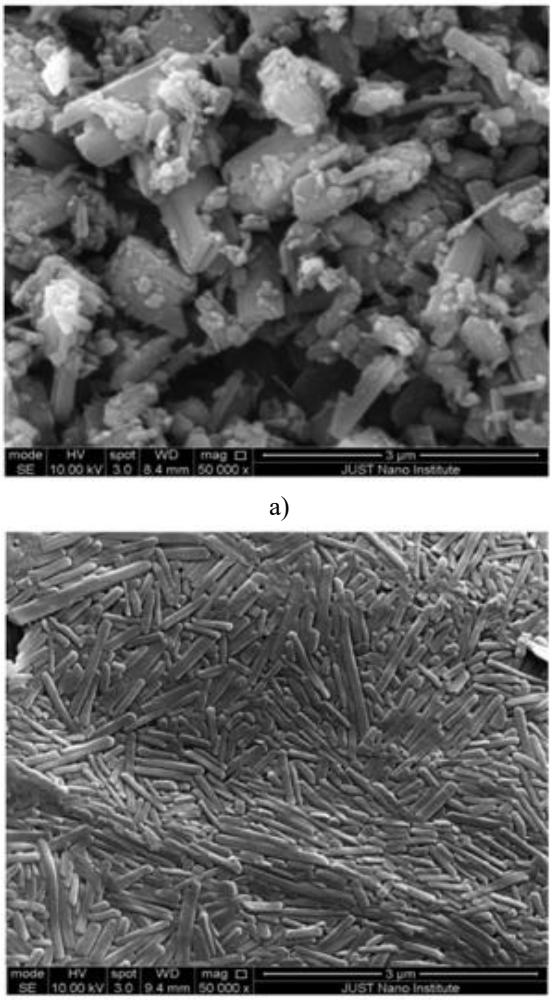

a)

b)

Figure 9. Scanning electron micrographs of (**a**) pure TDA and (**b**) TDA NCs F11.

Effects of aging

The long-term stability of TDA nanocrystals (F11) was investigated by tracking variations in particle size, polydispersity index (PDI), and solubility over a 90-day period. Measurements were taken on days 1, 30, 60, and 90, with samples stored under three different temperature conditions: 4 ± 0.5 °C, 25 ± 0.5 °C, and 40 ± 0.5 °C. On the first day, the nanocrystals had an average particle size of 181.6 ± 12 nm and a PDI of 0.23 ± 0.014. The initial saturation solubility of F11 was recorded as 9.63 ± 0.37 µg/mL. **Table 2** presents the detailed findings of particle size, PDI, and solubility for F11 under the various storage conditions and time points.

Table 2. Particle size, PDI, and saturation solubility of stored F11 at days 1, 30, 60, and 90 after storage at room temperature 25 ± 0.5 °C and accelerated conditions 4 ± 0.5 °C and 40 ± 0.5 °C.

Storage Condition	Parameters	Day 1	Day 30	Day 60	Day 90
–	**Particle size** (nm)	181.6 0 ± 12.00	–	–	–
	PDI	0.23 ± 0.01			
	Solubility (µg/mL)	9.63 ± 0.37			
4 ± 0.5 °C	**Particle size** (nm)	–	184.00 ± 7.00	187.00 ± 6.00	196.00 ± 3.00
	PDI		0.27 ± 0.04	0.28 ± 0.04	0.29 ± 0.08
	Solubility (µg/mL)		9.11 ± 0.47	9.08 ± 0.36	9.10 ± 0.19
25 ± 0.5 °C	**Particle size** (nm)	–	190.00 ± 5.00	218.00 ± 6.00*	236.00 ± 15.00*

	PDI		0.28 ± 0.08	0.28 ± 0.04	0.27 ± 0.02*
	Solubility (µg/mL)		8.84 ± 0.36	8.90 ± 0.42	8.78 ± 0.23*
40 ± 0.5 °C	**Particle size** (nm)	–	287.00 ± 7.00*	296.00 ± 12.00*	306.00 ± 10.00*
	PDI		0.34 ± 0.03*	0.36 ± 0.05*	0.39 ± 0.08*
	Solubility (µg/mL)		8.29 ± 0.29*	8.14 ± 0.10*	8.11 ± 0.19*

PDI: polydispersity index. *p-value < 0.05 compared to day 1.

Data from the long-term stability study revealed that F11 maintained its stability for up to three months when stored at 4 ± 0.5 °C, with no significant changes in particle size, PDI, or solubility as confirmed by unpaired t-test analysis. At 25 ± 0.5 °C, however, the particle size of the formulation showed a significant increase after 60 and 90 days. The PDI remained stable at days 30 and 60 but exhibited a significant rise by day 90. Solubility gradually declined over time, with a statistically significant decrease observed only at day 90.

Storage at 40 ± 0.5 °C had a pronounced impact on all measured parameters across the study period. Particle size increased by 1.58-, 1.63-, and 1.7-fold at days 30, 60, and 90, respectively. Concurrently, solubility decreased by 14%, 15.5%, and 15.8% at the corresponding time points, while PDI steadily increased throughout the three months.

Despite some initial flocculation observed in the second and third months at room temperature and during the first month under elevated temperature conditions, the nanoparticles of F11 retained their size within the nanoscale range. Importantly, they continued to provide enhanced solubility over the entire storage period.

Pharmacokinetics of pure TDA and TDA NCs

The plasma concentration–time profiles for both pure TDA and TDA nanocrystals (F11) following intranasal administration in SD rats are presented in **Figure 10**. Corresponding pharmacokinetic parameters are summarized in **Table 3**.

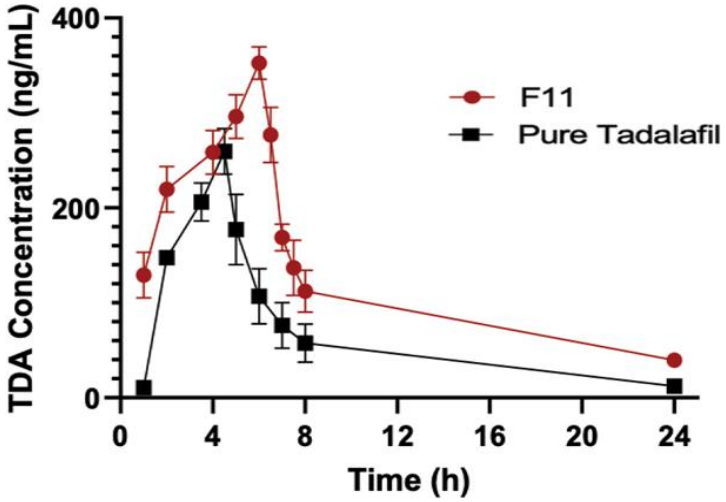

Figure 10. Plasma concentration–time curves of Tadalafil (TDA) after intranasal administration, comparing pure TDA (black squares) with TDA nanocrystals (F11; red circles). Data are expressed as mean ± SE (n = 4).

Table 3. The plasma pharmacokinetic parameters of pure TDA and TDA nanocrystals (TDA NCs) following intranasal administration in SD rats.

Parameter (unit)	TDA	TDA NCs	*p*-Value
C_{max} (ng/mL)	259.39 ± 49.65	352.77 ± 35.17*	0.0219
t_{max} (h)	4.50 ± 0.00	5.75 ± 0.50*	0.0025
λ_z (1/h)	0.26 ± 0.19	0.096 ± 0.017	0.1474
$t_{0.5}$ (h)	3.82 ± 2.10	7.37 ± 1.30*	0.0281
AUC_{0}^{∞} (ng. h/mL)	1492.37 ± 335.85	3377 ± 558*	0.0012
$AUMC_{0}^{\infty}$ (ng.h^2/mL)	11431.00 ± 2930.00	37822 ± 10858*	0.0045

MRT (h)	7.66 ± 1.11	11.07 ± 1.90*	0.0211
V_z / ***F*** **(mL/Kg)**	16.1 ± 11.6	12.7 ± 1.8	0.5802
CL / ***F*** (mL/Kg/h)	2.8 ± 0.0007	1.2 ± 0.2*	0.0059

TDA: pure tadalafil, TDA NCs: tadalafil nanocrystals, Data: mean ± SD (n = 4). *p-value < 0.05, compared to the pure TDA.

The pharmacokinetic evaluation of TDA NCs (F11) revealed a significant increase ($p < 0.05$) in Cmax, AUC0∞, AUMC0∞, MRT, tmax, and t0.5, showing 1.4-, 2.3-, 3.3-, 1.4-, 1.3-, and 1.93-fold enhancements, respectively, compared to pure TDA. Conversely, the apparent clearance (CL/F) of TDA NCs decreased significantly ($p < 0.05$) by 57.14% relative to the unformulated drug. The elevated Cmax and AUC0∞ observed in vivo may be attributed to the improved solubility and dissolution of TDA when formulated as nanocrystals, resulting in greater absorption. This effect is likely linked to the nanoscale and uniform particle size of TDA NCs, which enhances solubilization in aqueous media and promotes absorption across the thin nasal endothelial layer [57]. Additionally, the inclusion of PVA, a mucoadhesive polymer, likely prolongs nasal residence time and strengthens drug contact with the mucosa, thereby increasing local drug concentration [58], while also acting as a permeation enhancer to open tight junctions and facilitate mucosal absorption [59].

Interestingly, TDA NCs exhibited a longer tmax compared to pure TDA, a discrepancy requiring further investigation, as prior studies report variable results. For example, intranasal administration of celecoxib nanosuspension in rats led to a faster tmax compared to micron-sized particles, although AUC and Cmax remained unchanged [60]. Similarly, rufinamide NCs incorporated into a thermoresponsive nasal gel achieved a shorter tmax than the gel without nanocrystals [39]. Conversely, delayed tmax values, consistent with the present study, have been linked to slower drug release from NC formulations and lower free drug availability, influenced by the pH of the nasal cavity and the drug formulation [61].

Multiple studies have shown that nanoparticles can enhance bioavailability and plasma concentrations relative to the pure drug, often with delayed tmax, prolonged nasal retention, or slower absorption. For instance, L-Dopa-loaded chitosan nanoparticles demonstrated higher plasma levels and delayed tmax compared to the free drug, due to their positive charge increasing interaction with nasal mucosa and larger particle size prolonging residence and sustaining release [62]. Similarly, intranasal liposomal donepezil achieved higher plasma concentrations and longer tmax than the free drug, reflecting sustained release [63]. Solid lipid nanoparticles and nanostructured lipid carriers also improve nose-to-brain delivery by enhancing solubility and permeation, extending drug action, reducing enzymatic degradation, and prolonging mucosal residence time [64]. The mucoadhesive effect of PVA in TDA NCs likely contributes similarly to these outcomes, paralleling the effects of polymers such as HPMC and chitosan, which prolong retention and reduce mucociliary clearance [64].

Unexpectedly, oral administration studies, such as with cyadox nanosuspension, have shown delayed tmax due to lymphatic absorption, which prolongs systemic uptake [65], and while these findings were observed orally, nanoparticle interactions with nasal lymphatics may also influence intranasal pharmacokinetics [66]. Overall, the precise reason for the delayed tmax observed with TDA NCs remains unclear, warranting further investigation to determine whether it results from the NC components, interactions with nasal physiology, or alternative uptake and transport pathways compared to pure TDA.

Although the delayed tmax observed with TDA NCs compared to pure TDA may be considered a limitation for treating erectile dysfunction, where rapid onset is preferred, the prolonged duration of action associated with tadalafil could be advantageous [1]. This extended effect may also benefit other approved indications of TDA, such as pulmonary artery hypertension and benign prostatic hyperplasia [67]. Moreover, maintaining a sustained high concentration of TDA in the nasal cavity could enhance therapeutic efficacy for erectile dysfunction, potentially increasing patient and partner satisfaction [3]. The higher MRT of TDA NCs likely results from prolonged adhesion of the nanocrystals to the nasal mucosa, an effect attributed to PVA, which promotes particle attachment and sustained release over time, thereby increasing the MRT compared to pure TDA [68].

When compared with oral administration of aqueous TDA suspension reported in the literature, the Cmax and AUC0∞ were 410 ± 120 ng/mL and 4000 ± 1800 ng·h/mL, respectively, higher than values observed with nasal TDA, likely due to the larger dose (1.25-fold) used orally. However, t0.5 (3.9 ± 1.2 h) and MRT (8.8 ± 2.2 h) were consistent with the present findings, while the oral tmax (5.5 ± 1 h) was longer, reflecting the faster absorption characteristic of the nasal route [69–71]. To date, no studies have reported the pharmacokinetics of pure TDA administered intravenously or via inhalation. Teymouri Rad *et al*. (2019) evaluated TDA nanocomposites as a dry powder inhalation (10 mg/kg), reporting Cmax of 721.7 ± 222.4 ng/mL, AUC0∞ of 11.9

± 3.2 μg·h/mL, t0.5 of 4.1 ± 0.9 h, MRT of 19.2 ± 4.5 h, and tmax of 19.7 ± 6.7 h; however, direct comparison with the current study is limited due to differences in formulation, dose, and administration route [72].

Although the safety of intranasal TDA was not assessed in this study, it is anticipated that TDA NCs may exhibit fewer side effects than pure TDA, as lower doses may achieve similar efficacy. Nasal administration also bypasses the gastrointestinal tract, potentially reducing GI-related adverse effects associated with oral dosing [67]. To the best of our knowledge, this study is the first to report pharmacokinetic data for intranasally administered TDA, suggesting a novel strategy to improve its efficacy in treating erectile dysfunction.

While definitive conclusions cannot yet be drawn, successful development, clinical validation, and regulatory approval of an intranasal TDA formulation could offer multiple clinical advantages over oral administration. Nasal delivery provides high permeability through the mucosa, enabling rapid absorption and faster onset of action [73], while avoiding first-pass hepatic metabolism, which enhances bioavailability and systemic exposure [74]. Additionally, nasal administration may reduce gastrointestinal complications, enable more rapid therapeutic effects [73, 74], and facilitate targeted delivery to specific tissues, including the central nervous system via the olfactory route [75]. Overall, intranasal TDA administration could improve bioavailability, reduce systemic side effects, and enhance targeted drug delivery, positioning it as a promising alternative to oral therapy for selected indications [76, 77].

Conclusion

In summary, TDA nanocrystals were successfully formulated using the sonoprecipitation technique to achieve effective particle size reduction. Nanoparticles stabilized with PVA demonstrated significantly smaller particle sizes compared to those using Tween 80 or Pluronic F68. The nanocrystal formulation markedly improved the saturation solubility and dissolution rate of TDA by reducing particle size. Several factors, particularly the type and optimal concentration of stabilizer relative to the drug amount, are critical during the preparation process. Following intranasal administration in rats, TDA NCs exhibited superior pharmacokinetic performance compared to pure TDA, enhancing both absorption and residence time. Consequently, intranasal delivery of TDA as nanocrystals represents a promising novel approach that may provide improved clinical outcomes in the treatment of erectile dysfunction.

Acknowledgments: None

Conflict of Interest: None

Financial Support: None

Ethics Statement: None

References

1. Huang SA, Lie JD. Phosphodiesterase-5 (PDE5) inhibitors in the management of erectile dysfunction. Pharmacy & Therapeutics. 2013;38(7):407–19.
2. Mostafa T. Useful implications of low-dose long-term use of PDE-5 inhibitors. Sex Med Rev. 2016 Jul; 4(3):270–84. doi:10.1016/j.sxmr.2015.12.005
3. Coward RM, Carson CC. Tadalafil in the treatment of erectile dysfunction. Ther Clin Risk Manag. 2008 Dec; 4(6):1315–30. doi:10.2147/TCRM.S3336
4. Maiorino MI, Bellastella G, Esposito K. Diabetes and sexual dysfunction: current perspectives. Diabetes Metab Syndr Obes. 2014;7:95–105. doi:10.2147/DMSO.S36455
5. Shamloul R, Ghanem H. Erectile dysfunction. Lancet. 2013;381(9861):153–65. doi:10.1016/S0140-6736(12)60520-0
6. Burnett AL. The role of nitric oxide in erectile dysfunction: implications for medical therapy. J Clin Hypertens. 2006;8:53–62. doi:10.1111/j.1524-6175.2006.06026.x
7. Corbin JD, Francis SH, Webb DJ. Phosphodiesterase type 5 as a pharmacologic target in erectile dysfunction. Urology. 2002;60(2):4–11. doi:10.1016/S0090-4295(02)01686-2

8. Rad RT, Dadashzadeh S, Vatanara A, Alavi S, Ghasemian E, Mortazavi SA. Tadalafil nanocomposites as a dry powder formulation for inhalation: a new strategy for pulmonary arterial hypertension treatment. Eur J Pharm Sci. 2019;133:275–86. doi:10.1016/j.ejps.2019.04.001
9. Mudshinge SR, Deore AB, Patil S, Bhalgat CM. Nanoparticles: emerging carriers for drug delivery. Saudi Pharm J. 2011;19(3):129–41. doi:10.1016/j.jsps.2011.04.001
10. Dhumal RS, Biradar SV, Yamamura S, Paradkar AR, York P. Preparation of amorphous cefuroxime axetil nanoparticles by sonoprecipitation for enhancement of bioavailability. Eur J Pharm Biopharm. 2008;70(1):109–15. doi:10.1016/j.ejpb.2008.04.001
11. Iqbal P, Preece JA, Mendes PM. Nanotechnology: The "Top-Down" and "Bottom-Up" Approaches. In: Gale PA, Steed JW, editors. Supramolecular Chemistry: From Molecules to Nanomaterials. Chichester (UK): John Wiley & Sons; 2012. doi:10.1002/9780470661345
12. Salazar J, Müller RH, Möschwitzer JP. Combinative particle size reduction technologies for the production of drug nanocrystals. J Pharm (Cairo). 2014;2014(1):265754. doi:10.1155/2014/265754
13. Shegokar R, Müller RH. Nanocrystals: industrially feasible multifunctional formulation technology for poorly soluble actives. Int J Pharm. 2010;399:129–39. doi:10.1016/j.ijpharm.2010.07.044
14. Badr-Eldin SM, Elkheshen SA, Ghorab MM. Inclusion complexes of tadalafil with natural and chemically modified β-cyclodextrins. I: Preparation and in-vitro evaluation. Eur J Pharm Biopharm. 2008;70(3):819–27. doi:10.1016/j.ejpb.2008.06.024
15. Mehanna MM, Motawaa AM, Samaha MW. Insight into tadalafil–block copolymer binary solid dispersion: mechanistic investigation of dissolution enhancement. Int J Pharm. 2010;402(1-2):78–88. doi:10.1016/j.ijpharm.2010.09.024
16. Wlodarski K, Sawicki W, Paluch KJ, Tajber L, Grembecka M, Hawelek L, et al. The influence of amorphization methods on the apparent solubility and dissolution rate of tadalafil. Eur J Pharm Sci. 2014;62:132–40. doi:10.1016/j.ejps.2014.05.026
17. Zhang H-X, Wang J-X, Zhang Z-B, Le Y, Shen Z-G, Chen J-F. Micronization of atorvastatin calcium by antisolvent precipitation process. Int J Pharm. 2009;374(1–2):106–13. doi:10.1016/j.ijpharm.2009.02.015
18. Beck C, Dalvi SV, Dave RN. Controlled liquid antisolvent precipitation using a rapid mixing device. Chem Eng Sci. 2010;65(21):5669–75. doi:10.1016/j.ces.2010.04.001
19. Junyaprasert VB, Morakul B. Nanocrystals for enhancement of oral bioavailability of poorly water-soluble drugs. Asian J Pharm Sci. 2015;10(1):13–23. doi:10.1016/j.ajps.2014.08.005
20. Shete G, Jain H, Punj D, Prajapat H, Akotiya P, Bansal AK. Stabilizers used in nano-crystal based drug delivery systems. J Excipients Food Chem. 2016;5(4):184–209.
21. Fan M, Geng S, Liu Y, Wang J, Wang Y, Zhong J, et al. Nanocrystal technology as a strategy to improve drug bioavailability and antitumor efficacy. Curr Pharm Des. 2018;24(21):2416–24. doi:10.2174/1381612824666180515154109
22. Jahangir MA, Imam SS, Muheem A, Chettupalli A, Al-Abbasi FA, Nadeem MS, et al. Nanocrystals: characterization overview, applications in drug delivery, and toxicity concerns. J Pharm Innov. 2020;17(1):237–48. doi:10.1007/s12247-020-09499-1
23. Dizaj SM, Vazifehasl Z, Salatin S, Adibkia K, Javadzadeh Y. Nanosizing of drugs: effect on dissolution rate. Res Pharm Sci. 2015;10(2):95-108.
24. Kumar H, Mishra G, Sharma AK, Gothwal A, Kesharwani P, Gupta U. Intranasal drug delivery: A non-invasive approach for better delivery of neurotherapeutics. Pharm Nanotechnol. 2017;5(3):203–14. doi:10.2174/2211738505666170515113936
25. Upadhyay S, Parikh A, Joshi P, Upadhyay U, Chotai N. Intranasal drug delivery system – A glimpse to become maestro. J Appl Pharm Sci. 2011;1:34–44.
26. Wu C, Li B, Zhang Y, Chen T, Chen C, Jiang W, et al. Intranasal delivery of paeoniflorin nanocrystals for brain targeting. Asian J Pharm Sci. 2020;15(3):326–35. doi:10.1016/j.ajps.2019.11.002
27. Bojanapu A, Subramaniam AT, Munusamy J, Dhanapal K, Chennakesavalu J, Sellappan M, et al. Validation and method development of tadalafil in bulk and tablet dosage form by RP-HPLC. Drug Res. 2015;65(02):82–5. doi:10.1055/s-0034-1372608
28. Shen S, Wu Y, Liu Y, Wu D. High drug-loading nanomedicines: progress, current status, and prospects. Int J Nanomedicine. 2017;12:4085–109. doi:10.2147/IJN.S132780

29. Nair AB, Jacob S. A simple practice guide for dose conversion between animals and human. J Basic Clin Pharm. 2016;7(2):27–31. doi:10.4103/0976-0105.177703
30. Acharya SP, Pundarikakshudu K, Panchal A, Lalwani A. Preparation and evaluation of transnasal microemulsion of carbamazepine. Asian J Pharm Sci. 2013;8(1):64–70. doi:10.1016/j.ajps.2013.07.008
31. Erdő F, Bors LA, Farkas D, Bajza Á, Gizurarson S. Evaluation of intranasal delivery route for brain targeting. Brain Res Bull. 2018;143:155–70. doi:10.1016/j.brainresbull.2018.10.009
32. U.S. Food and Drug Administration. Q2(R2) Validation of Analytical Procedures. 2022. Available from: https://www.fda.gov/media/161201/download
33. Liu P, Viitala T, Kartal-Hodzic A, Liang H, Laaksonen T, Hirvonen J, et al. Interaction studies between indomethacin nanocrystals and PEO/PPO copolymer stabilizers. Pharm Res. 2015;32(2):628–39. doi:10.1007/s11095-014-1491-3
34. Tuomela A, Hirvonen J, Peltonen L. Stabilizing agents for drug nanocrystals: effect on bioavailability. Pharmaceutics. 2016;8(2):16. doi:10.3390/pharmaceutics8020016
35. Raghavan S, Trividic A, Davis A, Hadgraft J. Crystallization of hydrocortisone acetate: influence of polymers. Int J Pharm. 2001;212(2):213–21. doi:10.1016/S0378-5173(00)00610-4
36. Douroumis D, Fahr A. Stable carbamazepine colloidal systems using the cosolvent technique. Eur J Pharm Sci. 2007;30(5):367–74. doi:10.1016/j.ejps.2006.12.003
37. Lee M, Kim S, Ahn C-H, Lee J. Hydrophilic and hydrophobic amino acid copolymers for nano-comminution of poorly soluble drugs. Int J Pharm. 2010;384(1–2):173–80. doi:10.1016/j.ijpharm.2009.09.041
38. Jassim ZE, Hussein AA. Formulation and evaluation of clopidogrel tablet incorporating drug nanoparticles. Int J Pharm Sci. 2014;6(1):838–51.
39. Dalvi A, Ravi PR, Uppuluri CT. Design and evaluation of rufinamide nanocrystals loaded thermoresponsive nasal in situ gelling system for improved drug distribution to brain. Front Pharmacol. 2022;13:943772. doi:10.3389/fphar.2022.943772
40. Sinha B, Müller RH, Möschwitzer JP. Bottom-up approaches for preparing drug nanocrystals: formulations and factors affecting particle size. Int J Pharm. 2013;453(1):126–41. doi:10.1016/j.ijpharm.2013.01.019
41. Terayama H, Inada K, Nakayama H, Yasueda S, Esumi K. Preparation of stable aqueous suspension of a hydrophobic drug with polymers. Colloids Surf B Biointerfaces. 2004;39(4):159–64. doi:10.1016/j.colsurfb.2004.09.005
42. Dalvi SV, Dave RN. Controlling particle size of a poorly water-soluble drug using ultrasound and stabilizers in antisolvent precipitation. Ind Eng Chem Res. 2009;48(16):7581–93. doi:10.1021/ie900248f
43. Crowe LM, Reid DS, Crowe JH. Is trehalose special for preserving dry biomaterials? Biophys J. 1996;71(4):2087–93. doi:10.1016/S0006-3495(96)79407-9
44. Kabalnov A. Ostwald ripening and related phenomena. J Dispersion Sci Technol. 2001;22(1):1–12. doi:10.1081/DIS-100102675
45. Verma S, Gokhale R, Burgess DJ. Comparative study of top-down and bottom-up approaches for preparation of micro/nanosuspensions. Int J Pharm. 2009;380(1-2):216–22. doi:10.1016/j.ijpharm.2009.07.005
46. Khadka P, Ro J, Kim H, Kim I, Kim JT, Kim H, et al. Pharmaceutical particle technologies: an approach to improve drug solubility, dissolution and bioavailability. Asian J Pharm Sci. 2014;9(6):304–16. doi:10.1016/j.ajps.2014.05.005
47. Sun J, Wang F, Sui Y, She Z, Zhai W, Wang C, et al. Effect of particle size on solubility, dissolution rate, and oral bioavailability: evaluation using coenzyme Q10 as naked nanocrystals. Int J Nanomedicine. 2012;7:5733–44. doi:10.2147/IJN.S34365
48. Lee MK, Kim MY, Kim S, Lee J. Cryoprotectants for freeze drying of drug nano-suspensions: effect of freezing rate. J Pharm Sci. 2009;98(12):4808–17. doi:10.1002/jps.21786
49. Sharma PK, Sharma PK, Darwhekar GN, Birendra S. Formulation and evaluation of solid dispersion of tadalafil. Int J Drug Regul Aff. 2018;6(1):26–34. doi:10.22270/ijdra.v6i1.224
50. Omkaram I, Chakradhar RS, Rao JL. EPR, optical, infrared and Raman studies of VO2+ ions in polyvinylalcohol films. Physica B. 2007;388(1-2):318–25. doi:10.1016/j.physb.2006.06.134
51. Bhokare PL, Kendre PN, Pande VV. Design and characterization of nanocrystals of tadalafil for solubility and dissolution rate enhancement. Inventi Impact Pharm Process Dev. 2015;2015:1–7.
52. Athokpam B, Ramesh SG, McKenzie RH. Effect of hydrogen bonding on the infrared absorption intensity of OH stretch vibrations. Chem Phys. 2017;488–9:43–54. doi:10.1016/j.chemphys.2017.03.006

53. Butarbutar MET, Wathoni N, Wardhana YW. Characterization methods of amorphous form stability in solid dispersion: a review. Indones J Pharmaceutics. 2020;2(2):55–68. doi:10.24198/idjp.v2i2.27123
54. Zhu J, Li Q, Che Y, Liu X, Dong C, Chen X, et al. Effect of Na2CO3 on the microstructure and macroscopic properties of PVA/CMC composite film. Polymers. 2020;12(2):453. doi:10.3390/polym12020453
55. Rad RT, Mortazavi SA, Vatanara A, Dadashzadeh S. Enhanced dissolution rate of tadalafil nanoparticles prepared by sonoprecipitation technique: optimization and physicochemical investigation. Iran J Pharm Res. 2017;16(4):1335–48.
56. Aziz SB, Abdulwahid RT, Rasheed MA, Abdullah OG, Ahmed HM. Polymer blending as a novel approach for tuning the SPR peaks of silver nanoparticles. Polymers. 2017;9(10):486. doi:10.3390/polym9100486
57. Clementino AR, Pellegrini G, Banella S, Colombo G, Cantù L, Sonvico F, et al. Structure and fate of nanoparticles designed for the nasal delivery of poorly soluble drugs. Mol Pharm. 2021;18(8):3132–46. doi:10.1021/acs.molpharmaceut.1c00366
58. Chowdary KPR, Rao YS. Mucoadhesive microspheres for controlled drug delivery. Biol Pharm Bull. 2004;27(11):1717–24. doi:10.1248/bpb.27.1717
59. Abd El-Hameed M, Kellaway I. Preparation and in vitro characterisation of mucoadhesive polymeric microspheres as intranasal delivery systems. Eur J Pharm Biopharm. 1997;44(1):53–60. doi:10.1016/S0939-6411(97)00101-X
60. Zode S, Patil R, Gupta P, Jaladi R, Gautam A, Raghuvanshi R. Assessment of nanosuspension formulation for intranasal administration. Pharm Technol. 2020;44(9):36–43.
61. Morgen M, Bloom C, Beyerinck R, Bello A, Song W, Wilkinson K, et al. Polymeric nanoparticles for increased oral bioavailability and rapid absorption using celecoxib as a model of a low-solubility, high-permeability drug. Pharm Res. 2012;29(2):427–40. doi:10.1007/s11095-011-0558-7
62. Ahmad MZ, Sabri AH, Anjani QK, Domínguez-Robles J, Abdul Latip N, Hamid KA, et al. Design and development of levodopa loaded polymeric nanoparticles for intranasal delivery. Pharmaceuticals. 2022;15(3):370. doi:10.3390/ph15030370
63. Al Asmari AK, Ullah Z, Tariq M, Fatani A. Preparation, characterization, and in vivo evaluation of intranasally administered liposomal formulation of donepezil. Drug Des Dev Ther. 2016;10:205–15. doi:10.2147/DDDT.S93937
64. Nguyen T-T-L, Maeng H-J. Pharmacokinetics and pharmacodynamics of intranasal solid lipid nanoparticles and nanostructured lipid carriers for nose-to-brain delivery. Pharmaceutics. 2022;14(3):572. doi:10.3390/pharmaceutics14030572
65. Sattar A, Chen D, Jiang L, Pan Y, Tao Y, Huang L, et al. Preparation, characterization and pharmacokinetics of cyadox nanosuspension. Sci Rep. 2017;7(1):2289. doi:10.1038/s41598-017-02523-4
66. Lee J, Kang S, Park H, Sun JG, Kim EC, Shim G. Nanoparticles for lymph node-directed delivery. Pharmaceutics. 2023;15(2):565. doi:10.3390/pharmaceutics15020565
67. Van Driel M. Phosphodiesterase inhibitors: effectiveness and new applications. Ned Tijdschr Geneeskd. 2006;150:1613–6.
68. Leone F, Cavalli R. Drug nanosuspensions: a ZIP tool between traditional and innovative pharmaceutical formulations. Expert Opin Drug Deliv. 2015;12(10):1607–25. doi:10.1517/17425247.2015.1043886
69. Krupa A, Descamps M, Willart JF, Strach B, Wyska E, Jachowicz R, et al. High-energy ball milling as a green process to vitrify tadalafil and improve bioavailability. Mol Pharm. 2016;13(11):3891–902. doi:10.1021/acs.molpharmaceut.6b00688
70. Krupa A, Cantin O, Strach B, Wyska E, Tabor Z, Siepmann J, et al. In vitro and in vivo behavior of ground tadalafil hot-melt extrudates: carrier material determining rapid or controlled drug release. Int J Pharm. 2017;528(1-2):498–510. doi:10.1016/j.ijpharm.2017.05.057
71. Keller L-A, Merkel O, Popp A. Intranasal drug delivery: opportunities and toxicologic challenges during drug development. Drug Deliv Transl Res. 2021;12(4):735–57. doi:10.1007/s13346-020-00891-5
72. Rad RT, Dadashzadeh S, Vatanara A, Alavi S, Ghasemian E, Mortazavi SA, et al. Tadalafil nanocomposites as a dry powder formulation for inhalation. Eur J Pharm Sci. 2019;133:275–86. doi:10.1016/j.ejps.2019.04.001
73. Ghori MU, Mahdi Aljeboury MH, Smith AM, Conway BR. Nasal drug delivery systems: an overview. Am J Pharm Sci. 2015;3(5):110–9.

74. Amponsah SK, Adams I. Drug absorption via the nasal route: opportunities and challenges. In: Pathak YV, Yadav HKS, editors. Nasal Drug Delivery: Formulations, Developments, Challenges, and Solutions. Cham: Springer; 2023. p. 25–42. doi:10.1007/978-3-031-23112-4_3
75. Dhuria SV, Hanson LR, Frey WH II. Intranasal delivery to the central nervous system: mechanisms and experimental considerations. J Pharm Sci. 2010;99(4):1654–73. doi:10.1002/jps.21924
76. Pires A, Fortuna A, Alves G, Falcão A. Intranasal drug delivery: how, why, and what for? J Pharm Pharm Sci. 2009;12:288–311. doi:10.18433/J3NC79
77. Kim JS, Kim MS, Baek IH. Enhanced bioavailability of tadalafil after intranasal administration in beagle dogs. Pharmaceutics. 2018;10(4):187. doi:10.3390/pharmaceutics10040187